Dislocation Defect Layer-Induced Magnetic Bi-states Phenomenon in Epitaxial $La_{0.7}Sr_{0.3}MnO_3$ (111) Thin Films

Yanan Zhao [#a], Yaojin Li [#a], Chen Chen [a], Guohua Dong [a], Shukai Zhu [a], Yifan Zhao [a], Bian Tian [b], Zhuangde Jiang [b], Ziyao Zhou [a], Keqing Shi [c], Ming Liu [a], Jingye Pan [c]**

a Electronic Materials Research Laboratory, Key Laboratory of the Ministry of Education, School of Electronic and Information Engineering, State Key Laboratory for Mechanical Behavior of Materials, International Joint Laboratory for Micro/Nano Manufacturing and Measurement Technology, Xi'an Jiaotong University (Yantai) Research Institute For Intelligent Sensing Technology and System, Xi'an Jiaotong University, Xi'an 710049, China

b State Key Laboratory for Manufacturing Systems Engineering, Collaborative Innovation Center of High-End Manufacturing Equipment, the International Joint Laboratory for Micro/Nano Manufacturing and Measurement Technology, Xi'an Jiaotong University, Xi'an 710049, China

c Department of Intensive Care, Precision Medicine Center Laboratory, The First Affiliated Hospital of Wenzhou Medical University, Wenzhou 325000, China

E-mail: mingliu@xjtu.edu.cn

E-mail: panjingye@wzhospital.cn

#there authors contribute equally

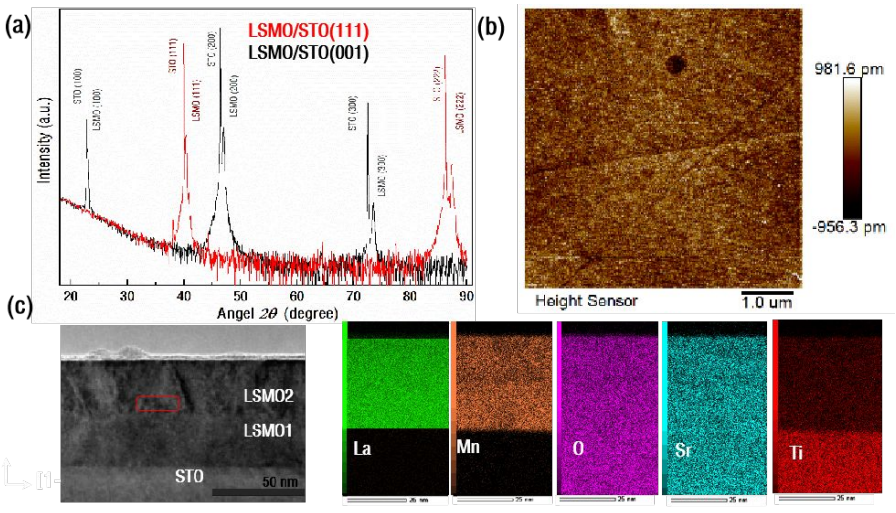

Figure S1. (a) XRD patterns of LSMO thin films on STO (001), (111) substrates. The

red line is for LSMO/STO (111) thin films, and the black line is for LSMO/STO(001) thin films. (b) The surface morphology of LSMO/STO (111) thin films. (c) TEM image of LSMO/STO (111) thin films and EELS chemical mapping extracted from La, Mn, Sr, O, and Ti.

Figure S1(a) shows (*00l*), (*lll*)-textured orientations of LSMO thin films along the (001) and (111) -oriented STO substrates. It also shows a good flatness of morphology in LSMO (111) thin films. The cross-sectional transmission electron microscopy image of other thickness LSMO (111) thin film, as shown in Figure S1(c), indicates an obvious double-layer structure divided by continuous dislocation defect arrays. In addition, the atomic chemical elemental maps supplied by electron energy loss spectroscopy (EELS), especially the Mn, O, and Sr maps, indicate a different bright intensity corresponding to the dislocation strain distribution revealed by HAADF. The structural dislocation defect arrays may cause the Mn and O chemical element of the LSMO2 sublayer to migrate towards the strain interface, which would affect the magnetic property.

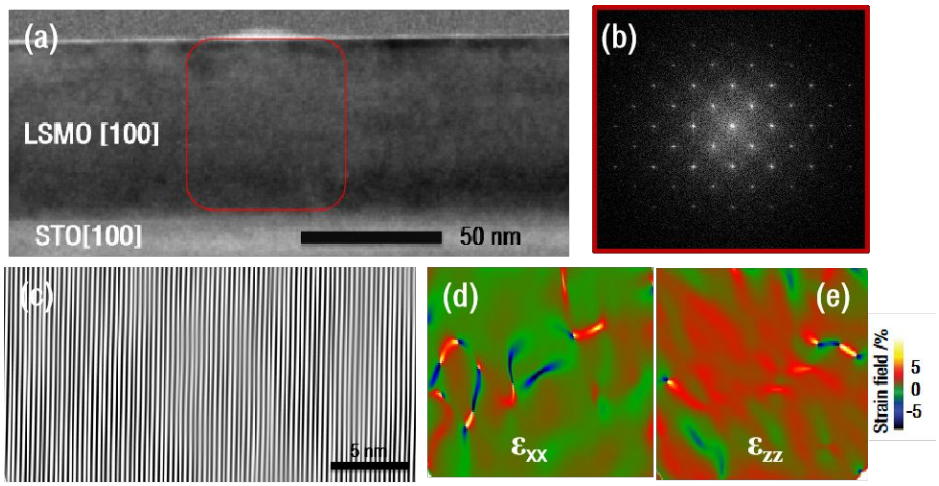

Figure S2.(a) Low magnification bright field of LSMO (100) cross-section.(b) A selected area diffraction pattern was obtained from LSMO (100) selected by a red box. (c) The Fourier transformation image of Figure R2(b). (d) The calculated ε_{xx} strain fields by using the GPA method. (e) The calculated ε_{zz} strain fields by using the GPA method.

We have deposited the similar thickness of LSMO (100) films and added the

geometric phase analysis (GPA) and Fourier transform of LSMO (100) films, as shown in Figures S2. Obviously, Figure S2 (a) and S2 (b) show no continuous dislocation defect arrays and spot splitting. And it also presents a homogeneous strain distribution along *x, z* axis in Figure S2(d) and S2(e).

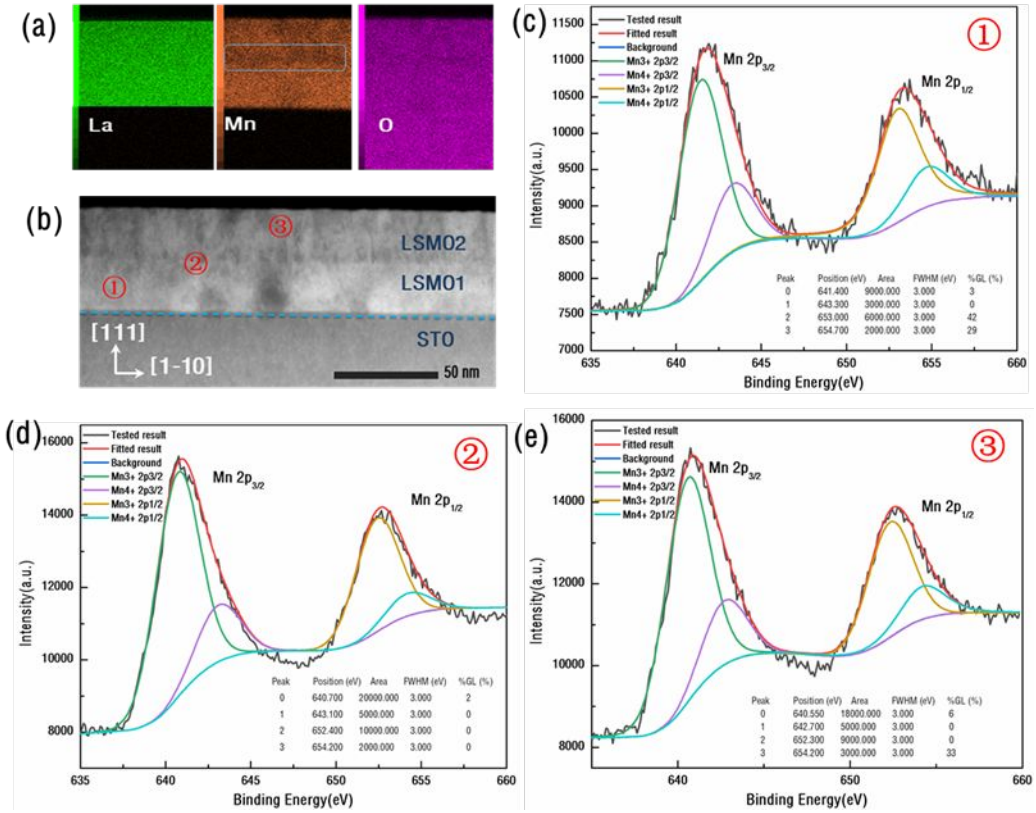

Figure S3. (a) The EELS chemical mapping extracted from La, Mn and O. (b) TEM image of LSMO/STO (111) thin films. (c) XPS spectrum of LSMO1 layer. (d) XPS spectrum of the dislocation layer. (e) XPS spectrum of LSMO2 layer.

For further analysis of the factors that affect the magnetic property, the surface concentration of Mn^{3+}/Mn^{4+} of in LSMO1, LSMO2 and the dislocation layers of LSMO (111) films were measured by XPS spectra, respectively. The ratio of Mn^{3+}/Mn^{4+} in the dislocation layer is 4.028, which is much larger than that of LSMO1, LSMO2 layers. And the Mn^{3+}/Mn^{4+} ratio (3.0) of the LSMO1 layer is very close to 3.1 of the LSMO2 thin films. Here, Mn^{3+}/Mn^{4+} electronic distribution is not uniform in thick LSMO (111) films.Thus, the dislocation layer with the enhanced Mn^{3+} concentration may lead to the

super-exchange coupling between Mn^{3+}-Mn^{3+} sites along the surface normal direction, resulting in a net AF alignment between the FM regions in the strain interface.

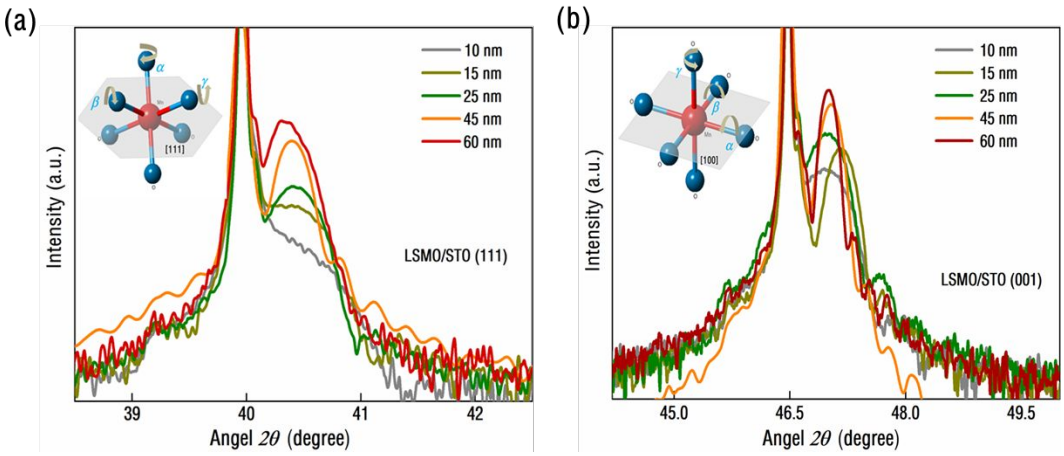

Figure S4. (a) The variation trend of a zoomed XRD of LSMO (111) thin films with varing thicknesses. (b) The variation trend of a zoomed XRD of LSMO (001) thin films with varing thicknesses.

There are different variation trends of XRD peak shape and position with the varing thickness of LSMO (111) and (001) thin films. Figure S4(a) shows that the interplanar spacing of LSMO (111) becomes larger, giving that the peak position becomes small as the increase of thickness. Figure S4(b) shows that the peak position of LSMO (001) gets larger and then decreases until it gets stabilization as the increase of thickness. It may induce different lattice deformations to result in the corresponding magnetic property and crystalline structure in manganese oxides.

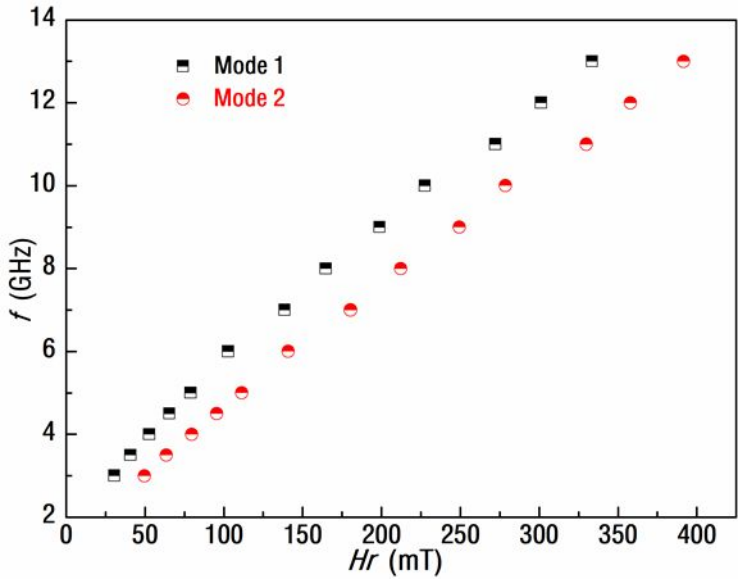

Figure S5. The FMR H_r dependence of frequency for FMR Mode1 and Mode2, respectively.

The variation of FMR H_r field as a function of frequency is shown in Figure S5, and the effective demagnetizing magnetization $4\pi M_{eff\text{-}1}$ (4637 Oe) of FMR Mode1 and $4\pi M_{eff\text{-}2}$ (2754 Oe) of FMR Mode 2 are obtained through Kittel equation[1, 2],

$$\frac{2\pi f}{\gamma} = \sqrt{(H_r + 4\pi M_{eff})H_r} \qquad \text{(S-1)}$$

where γ is the gyromagnetic ratio (~2.8 MHz/Oe), H_r is the FMR field, and M_{eff} is the effective demagnetizing magnetization.

References

1. Liu, M.; Zhou, Z.; Nan, T.; Howe, B. M.; Brown, G. J.; Sun, N. X., Voltage tuning of ferromagnetic resonance with bistable magnetization switching in energy-efficient magnetoelectric composites. *Adv. Mater.* **2013,** *25* (10), 1435-9.

2. Kittel, C., On the Theory of Ferromagnetic Resonance Absorption. *Physical Review* **1948,** *73* (2), 155-161.